Applied Catalysis B: Environmental 142–143 (2013) 249–258

Contents lists available at SciVerse ScienceDirect

Applied Catalysis B: Environmental

journal homepage: www.elsevier.com/locate/apcatb

HNO_3-involved one-step low temperature solvothermal synthesis of N-doped TiO_2 nanocrystals for efficient photocatalytic reduction of Cr(VI) in water

Yong Cai Zhang[a,b,*], Min Yang[a], Geshan Zhang[b], Dionysios D. Dionysiou[b,c,**]

[a] Key Laboratory of Environmental Material and Environmental Engineering of Jiangsu Province, School of Chemistry and Chemical Engineering, Yangzhou University, Yangzhou 225002, China
[b] Environmental Engineering and Science Program, 705 Engineering Research Center, University of Cincinnati, Cincinnati, OH 45221-0012, USA
[c] Nireas-International Water Research Centre, University of Cyprus, 20537 Nicosia, Cyprus

ARTICLE INFO

Article history:
Received 30 January 2013
Received in revised form 17 April 2013
Accepted 10 May 2013
Available online 18 May 2013

Keywords:
N-doped TiO_2
Nitric acid
Solvothermal
Photocatalytic reduction
Hexavalent chromium

ABSTRACT

A one-step low temperature (180 °C) solvothermal route, which utilized HNO_3 as the nitrogen source, was proposed for the synthesis of nanocrystalline N-doped TiO_2 (denoted as TiO_2-HNO_3). The structure, composition, BET specific surface area and optical properties of TiO_2-HNO_3 were characterized by X-ray diffraction, Fourier transform infrared spectroscopy, X-ray photoelectron spectroscopy, transmission electron microscopy, high resolution transmission electron microscopy, N_2 adsorption–desorption isotherms and UV–vis diffuse reflectance spectroscopy. The photocatalytic properties of TiO_2-HNO_3 were tested for the reduction of Cr(VI) in water under both UV and visible light ($\lambda > 420$ nm) irradiation, and compared with those of TiO_2-$NH_3{\cdot}H_2O$ (which was solvothermally synthesized using $NH_3{\cdot}H_2O$ as the nitrogen source) and TiO_2 P25. The photocatalytic results demonstrated that TiO_2-HNO_3 possessed much higher photocatalytic activity than TiO_2-$NH_3{\cdot}H_2O$ and TiO_2 P25 in the reduction of aqueous Cr(VI) under both UV and visible light ($\lambda > 420$ nm) irradiation, and the dosage of TiO_2-HNO_3 and the initial concentration of Cr(VI) aqueous solution had significant effects on the efficiency of Cr(VI) reduction. Besides, Cr(VI) was reduced to Cr(III) after the TiO_2-HNO_3-mediated photocatalytic reactions. The present work suggests that HNO_3 is a promising nitrogen source for low temperature solvothermal synthesis of nanocrystalline N-doped TiO_2, which can be applied as a visible light-activated photocatalyst in efficient utilization of solar energy for treating Cr(VI) wastewater.

1. Introduction

Cr(VI) is a common contaminant in the wastewaters arising from electroplating, pigments, mining and chromate manufacturing industries [1–13]. It is highly toxic and highly mobile in water, thus has been classified as a priority pollutant by many countries of the world [1–13]. A preferred approach for treating Cr(VI) in water is to reduce it to less toxic Cr(III), which can be precipitated as $Cr(OH)_3$ ($K_{sp}{}^{\theta}(Cr(OH)_3) = 6.3 \times 10^{-31}$) in neutral and alkaline solutions and removed as a solid waste [1–13]. Nevertheless, conventional chemical reduction methods need to use a large quantity of reducing agents (such as $FeSO_4$, $FeCl_2$, $NaHSO_3$ or SO_2 [13]), which are not cost-effective and can cause secondary pollution [13]. By contrast, semiconductor-mediated photocatalytic reduction of Cr(VI) has exceptional advantages, such as (i) low cost, (ii) direct use of "free", infinite, clean and safe solar energy, (iii) no use and no release of other undesirable chemicals, and (iv) reusability [1–13]. Hence, semiconductor-mediated photocatalytic reduction is widely recognized as a promising way for Cr(VI) wastewater treatment [1–13].

The development of high performance photocatalysts is indispensable for the application of the photocatalytic process to large-scale Cr(VI) wastewater treatment. TiO_2 is one of the few options of photocatalysts that are suitable for practical applications in water treatment, by virtue of its flexibility to catalyze numerous redox reactions, low cost, low toxicity, and good chemical and photochemical stability [14]. Unfortunately, pure TiO_2 has a major drawback stemming from its large band gap (3.0–3.2 eV [14]), which means it can absorb mainly UV light (UV light constitutes only ~5% of solar energy, whereas visible light makes

* Corresponding author at: Key Laboratory of Environmental Material and Environmental Engineering of Jiangsu Province, School of Chemistry and Chemical Engineering, Yangzhou University, Yangzhou 225002, China.
Tel.: +86 51487962581; fax: +86 51487975244.
** Corresponding author at: Environmental Engineering and Science Program, 705 Engineering Research Center, University of Cincinnati, Cincinnati, OH 45221-0012, USA.
E-mail addresses: zhangyc@yzu.edu.cn (Y.C. Zhang), dionysios.d.dionysiou@uc.edu (D.D. Dionysiou).

0926-3373/$ – see front matter © 2013 Elsevier B.V. All rights reserved.
http://dx.doi.org/10.1016/j.apcatb.2013.05.023

up ~46% of solar energy [15]). For overcoming this limitation, intensive research efforts have been recently focused on the modification of TiO_2 photocatalyst to enable its visible light response [14,17–38]. Among the modification methods developed, nonmetal doping of TiO_2 has demonstrated great potential in achieving the visible light-activated photocatalysis, while nitrogen is considered as the most promising dopant [14]. However, until now, N-doped TiO_2 has been mostly studied for photocatalytic degradation of organic compounds through the oxidative pathway [14,19–38]. To our knowledge, the available information on N-doped TiO_2-mediated photocatalytic reduction of Cr(VI) is still very limited [16–18].

The exploration of new synthesis methods and nitrogen sources for N-doped TiO_2 has great scientific and practical significance, because the properties of N-doped TiO_2 depend heavily on the synthesis methods and nitrogen sources employed [14,17–38]. To date, most of the methods developed for the synthesis of N-doped TiO_2 involve two successive steps [14]: first, preparation of TiON-containing precursors by sol–gel, coprecipitation, microemulsion, hydrothermal or solvothermal method, etc, then, calcination at 300–600 °C to produce N-doped TiO_2; or first, synthesis of TiO_2, then, doping it with nitrogen via sophisticated physical techniques (e.g., ion implantation and sputtering) or treatment in nitrogen-containing atmospheres at high temperatures. However, the two-step synthesis methods are often complicated, high temperature-demanding, time-consuming, relatively expensive, or even worse, hard to obtain high performance photocatalysts [14]. It is yet desirable to develop simple low temperature routes for synthesizing high performance N-doped TiO_2 photocatalyst. Besides, the nitrogen sources used hitherto for wet chemistry synthesis of N-doped TiO_2 are mostly $NH_3{\cdot}H_2O$, urea, aliphatic or aromatic amines [14,17–38]. As for HNO_3, it is by far rarely used as a nitrogen source for synthesizing N-doped TiO_2. But undeniably, the adoption of HNO_3 as a nitrogen source for synthesizing N-doped TiO_2 may present some new or special features. For example, unlike the widely used alkaline nitrogen sources (e.g., $NH_3{\cdot}H_2O$, urea, aliphatic or aromatic amines) which can promote the hydrolysis of titanium precursors, HNO_3 can instead restrain the hydrolysis of titanium precursors, which will facilitate the homogeneous doping process and formation of smaller-sized product.

Solvothermal method not only enables obtaining materials with large surface area and high crystallinity, but is also capable of incorporating hybrid atoms in the lattices of the target materials at considerably low temperatures [35–38]. Herein, a one-step low temperature (180 °C) solvothermal route, which uses HNO_3, tetrabutyl titanate and ethanol (which can dissolve tetrabutyl titanate and is the most common and cheapest organic solvent) as the nitrogen source, TiO_2 precursor and solvent, respectively, was proposed to synthesize nanocrystalline N-doped TiO_2 (TiO_2-HNO_3). The photocatalytic properties of TiO_2-HNO_3 were tested for the reduction of Cr(VI) in water under both UV and visible light ($\lambda > 420$ nm) irradiation, and compared with those of TiO_2-$NH_3{\cdot}H_2O$ and TiO_2 P25.

2. Experimental

HNO_3 (65.0–68.0% or 14.36–15.16 mol/L), $NH_3{\cdot}H_2O$ (25.0–28.0% or 13.32–14.44 mol/L) and absolute ethanol (EtOH, ≥99.7%) were of analytical grade, tetrabutyl titanate (TBT, ≥98.0%) was of chemical grade, potassium dichromate ($K_2Cr_2O_7$) was of guaranteed grade (≥99.8%), 100 mg/L $K_2Cr_2O_7$ aqueous solution (pH 5.2) was prepared by dissolving 1.0 g of $K_2Cr_2O_7$ in 10.0 L of deionized water, and lower concentrations (75, 50 and 25 mg/L) of $K_2Cr_2O_7$ aqueous solutions were prepared by proper dilution of the 100 mg/L $K_2Cr_2O_7$ aqueous solution with deionized water.

2.1. Synthesis

Thirty-nine mL of EtOH and 1.0 mL of HNO_3 were placed into a 50 mL Teflon-lined stainless steel autoclave, and stirred for 10 min to blend them. Then, 2.0 mL of TBT was added to the EtOH–HNO_3 solution and stirred for 20 min, and a pale yellow homogeneous solution was formed. The autoclave was sealed and heated in an electric oven at 180 °C for 12 h. After the autoclave naturally cooled to room temperature, the resultant yellow precipitate was centrifuged after discarding the upper solution, washed with EtOH and deionized water, and dried in vacuum at 100 °C for 4 h.

For comparison, TiO_2-$NH_3{\cdot}H_2O$ was also solvothermally synthesized using the same procedures and conditions, except HNO_3 was replaced by $NH_3{\cdot}H_2O$.

It is also worth mentioning that for safety, the amount of HNO_3 used for the solvothermal synthesis had better not exceed 3.0 mL (when 4.0 mL of HNO_3 was used, the Teflon liner of our autoclave deformed and the reaction solution leaked). Furthermore, the products synthesized using 2.0–3.0 mL of HNO_3 and 2.0–3.0 mL $NH_3{\cdot}H_2O$ exhibited lower photocatalytic activities than those synthesized using 1.0 mL of HNO_3 and 1.0 mL $NH_3{\cdot}H_2O$, respectively. Therefore, the present work only deals with the results of TiO_2-HNO_3 and TiO_2-$NH_3{\cdot}H_2O$, which were synthesized using 1.0 mL of HNO_3 and $NH_3{\cdot}H_2O$, respectively.

2.2. Characterization

The obtained products were characterized by powder X-ray diffraction (XRD, German Bruker AXS D8 ADVANCE X-ray diffractometer), Fourier transform infrared spectroscopy (FTIR, American Varian Cary 670 FT-IR spectrometer), X-ray photoelectron spectroscopy (XPS, American Thermo-VG Scientific ESCALAB 250 XPS system, Al K_α radiation and adventitious C 1s peak (284.6 eV) calibration), transmission electron microscopy (TEM, The Netherlands Philips Tecnai-12 transmission electron microscopy), high resolution transmission electron microscopy (HRTEM, American FEI Tecnai G^2 F30 S-TWIN field-emission transmission electron microscopy), N_2 adsorption–desorption isotherms (American Micromeritics Instrument Corporation TriStar II 3020 surface area and porosity analyzer), and UV–vis diffuse reflectance spectra (American Varian Cary 5000 UV–Vis-NIR spectrophotometer).

2.3. Photocatalytic tests

The photocatalytic properties of TiO_2-HNO_3 as well as TiO_2-$NH_3{\cdot}H_2O$ and TiO_2 P25 were tested for the reduction of Cr(VI) in water under both UV (high pressure mercury lamp) and visible light ($\lambda > 420$ nm) irradiation in custom-made photochemical reactors (Electronic Supplementary Materials, Figs. S1 and S2). Prior to illumination, 300 mL of 25–100 mg/L $K_2Cr_2O_7$ aqueous solution containing 0.2–0.6 g of photocatalyst was magnetically stirred in the dark for 60 min. During illumination, about 3 mL of suspension was taken from the reactor at a scheduled interval and filtered with pore size = 0.22 μm cellulose acetate membrane filters to separate the photocatalyst. The Cr(VI) content in the filtrate was determined colorimetrically at 540 nm using the standard diphenylcarbazide method.

3. Results and discussion

Fig. 1(a) and (b) shows the XRD patterns of TiO_2-$NH_3{\cdot}H_2O$ and TiO_2-HNO_3, respectively. Both of them display only the XRD peaks characteristic of anatase TiO_2 (JCPDS card no. 21-1272). Using the Scherrer formula ($D_{hkl} = K\lambda/\beta\cos\theta$, where D is the crystallite size in the direction perpendicular to ($h\,k\,l$) crystal plane (nm); K is a dimensionless shape factor whose value is taken as 0.89 here; λ is

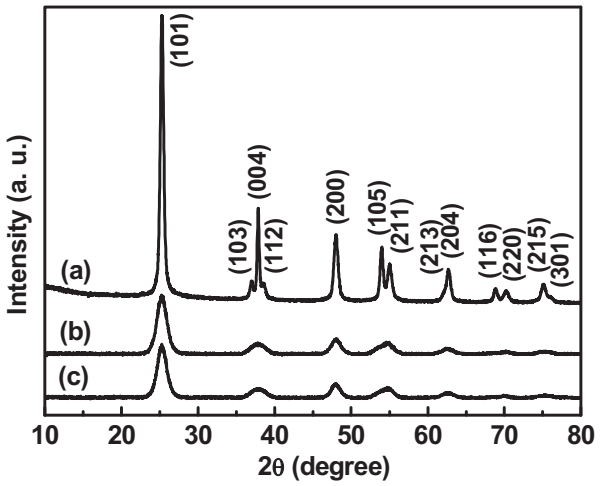

Fig. 1. XRD patterns of (a) TiO_2-NH_3·H_2O, (b) TiO_2-HNO_3 and (c) TiO_2-HNO_3-AU (the recovered TiO_2-HNO_3 after use in the photocatalytic reduction of Cr(VI)).

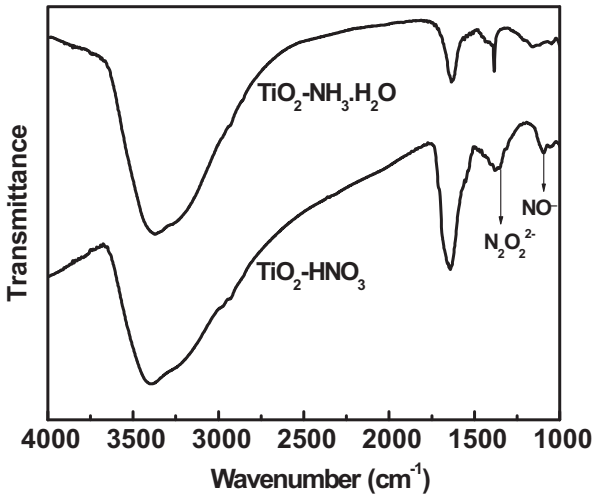

Fig. 2. FTIR spectra of TiO_2-NH_3·H_2O and TiO_2-HNO_3.

the X-ray wavelength (Cu Kα1 = 0.15406 nm); β is the full width at half maximum (FWHM) of ($h\,k\,l$) diffraction peak after subtracting the instrumental broadening (rad); and θ is the Bragg angle (rad)) based on the FWHM of (1 0 1) diffraction peak in their XRD patterns [32,33], the crystallite sizes of TiO_2-NH_3·H_2O and TiO_2-HNO_3 were estimated to be 16 and 5 nm, respectively. The difference in the crystallite sizes of TiO_2-NH_3·H_2O and TiO_2-HNO_3 is probably due to their different formation mechanisms. In the presence of NH_3·H_2O, the formation of TiO_2 might be mainly via a two-step process: first hydrolysis of TBT into TiO_2·xH_2O (as can be inferred from the fact that the addition of TBT to the NH_3·H_2O–EtOH solution immediately produced a colloidal suspension) [39], then condensation of TiO_2·xH_2O under the 180 °C solvothermal condition to TiO_2. On the other hand, in the presence of HNO_3, TiO_2 might be formed mainly via the thermolysis of TBT under the 180 °C solvothermal condition, because concentrated HNO_3 (65.0–68.0%) could suppress the hydrolysis of TBT (as can be inferred from the fact that the addition of TBT to the HNO_3–EtOH solution only produced a homogeneous solution) and the crystallite size of TiO_2-HNO_3 was close to that (about 2–6 nm) of the TiO_2 product obtained via solvothermal decomposition of TBT in pure ethanol at 180 °C for 12 h. Besides, the decomposition and reduction of concentrated HNO_3 (65.0–68.0%) under the current solvothermal condition would generate NO, NO_2, and even other NO species:

$$2HNO_3 + 3CH_3CH_2OH \rightarrow 3CH_3CHO + 2NO\,(\text{or other NO species}) + 4H_2O$$

$$4HNO_3 \rightarrow 4NO_2 + O_2 + 2H_2O$$

$$3NO_2 + H_2O \rightarrow 2HNO_3 + NO$$

The NO species could be chemisorbed on the surface or incorporated into the lattices of the resultant TiO_2 nanocrystals [40], giving rise to NO-modified TiO_2. This was later confirmed by FTIR and XPS analysis of TiO_2-HNO_3.

Fig. 2 shows the FTIR spectra of TiO_2-NH_3·H_2O and TiO_2-HNO_3 in the wavenumber range of 1000–4000 cm^{-1}. Both products display obvious absorption peaks around 3000–3660, 1630, 1382 and 1050 cm^{-1}. The broad absorption band around 3000–3660 cm^{-1} and the peak at about 1630 cm^{-1} are related to the surface —OH (and also —NH for TiO_2-NH_3·H_2O) and adsorbed H_2O of TiO_2 [22]. The peaks around 1382 and 1050 cm^{-1} are indicative of C—H and C—O from residual organic contaminants [41]. However, compared to TiO_2-NH_3·H_2O, TiO_2-HNO_3 exhibits new IR absorption peaks around 1348 and 1100 cm^{-1} which imply the presence of $N_2O_2^{2-}$ and NO^- [40,42–45].

The surface elemental constituents and valence states of TiO_2-NH_3·H_2O and TiO_2-HNO_3 were determined by XPS, and the obtained results are shown in Fig. 3 and Table 1. The survey XPS spectra of TiO_2-NH_3·H_2O and TiO_2-HNO_3 (Fig. 3) reveal that they consist of Ti, O, N and C elements. From the high resolution XPS spectra of Ti 2p (Fig. 3), it can be seen that both TiO_2-NH_3·H_2O and TiO_2-HNO_3 contain a single Ti species with the Ti $2p_{3/2}$ binding energy at 458.5 eV, which correspond to Ti(IV) in TiO_2 [46]. On the other hand, from the high resolution XPS spectra of O 1s, N 1s and C 1s (Fig. 3), it can be seen that these three constituents of TiO_2-NH_3·H_2O and TiO_2-HNO_3 comprise multiple oxidation states, and thus peak-fitting was performed. The O 1s XPS spectra of TiO_2-NH_3·H_2O and TiO_2-HNO_3 display three peaks at (i) 529.7 and 529.8, (ii) 531.0 and 531.2, and (iii) 532.2 and 532.3 eV (Fig. 3), which can be attributed to (i) lattice oxygen of anatase TiO_2, (ii) Ti—ON or C═O, and (iii) —OH or C—O [46–48], respectively. The C 1s XPS spectra of TiO_2-NH_3·H_2O and TiO_2-HNO_3 display three peaks around (i) 284.6 and 284.6, (ii) 286.0 and 286.0, and (iii) 288.3 and 288.2 eV (Fig. 3), which can be assigned to (i) C—C or C—H, (ii) C—O, and (iii) C═O [46], respectively. It is noteworthy that there is no peak around 281–282 eV in the XPS spectra of C 1s (Fig. 3), excluding the formation of Ti—C bonds by substituting carbon for oxygen anions in the anatase lattices [46].

The N 1s XPS spectra of TiO_2-NH_3·H_2O and TiO_2-HNO_3 display two peaks at (i) 399.2 and 400.2, and (ii) 400.6 and 401.6 eV (Fig. 3), respectively. The occurrence of the N 1s peak at 399–402 eV was common to N-doped TiO_2 [14,19–38,41–49]. However, the assignments of such N 1s peak were varied (e.g., it has been assigned to NH_3, NH_x, O—Ti—N, NO^- (e.g., Ti—ON or Ti—NO), $N_2O_2^{2-}$, NO_2^-, N_2 and NO, etc. at the interstitial sites or surface of TiO_2 crystals), depending on the nitrogen sources, synthesis methods and

Table 1
The physicochemical characteristics of TiO_2-HNO_3, TiO_2-NH_3·H_2O and TiO_2 P25. *Note*: the nitrogen contents of TiO_2-HNO_3 and TiO_2-NH_3·H_2O were calculated by reference to their respective titanium contents; the superscript ^{S} and ^{T} denote the sizes derived from Scherrer formula and TEM images, respectively; and SSA = specific surface area.

Name	N/Ti (at%)	Size (nm)	BET SSA (m^2/g)
TiO_2-HNO_3	5.0(Ti-ON) and 1.2($N_2O_2^{2-}$)	5^S, 4–6^T	208.1
TiO_2-NH_3·H_2O	1.1(Ti-NH_3) and 0.8(NH_4^+)	16^S, 14–18^T	87.1
TiO_2 P25	0	16–28^T	50

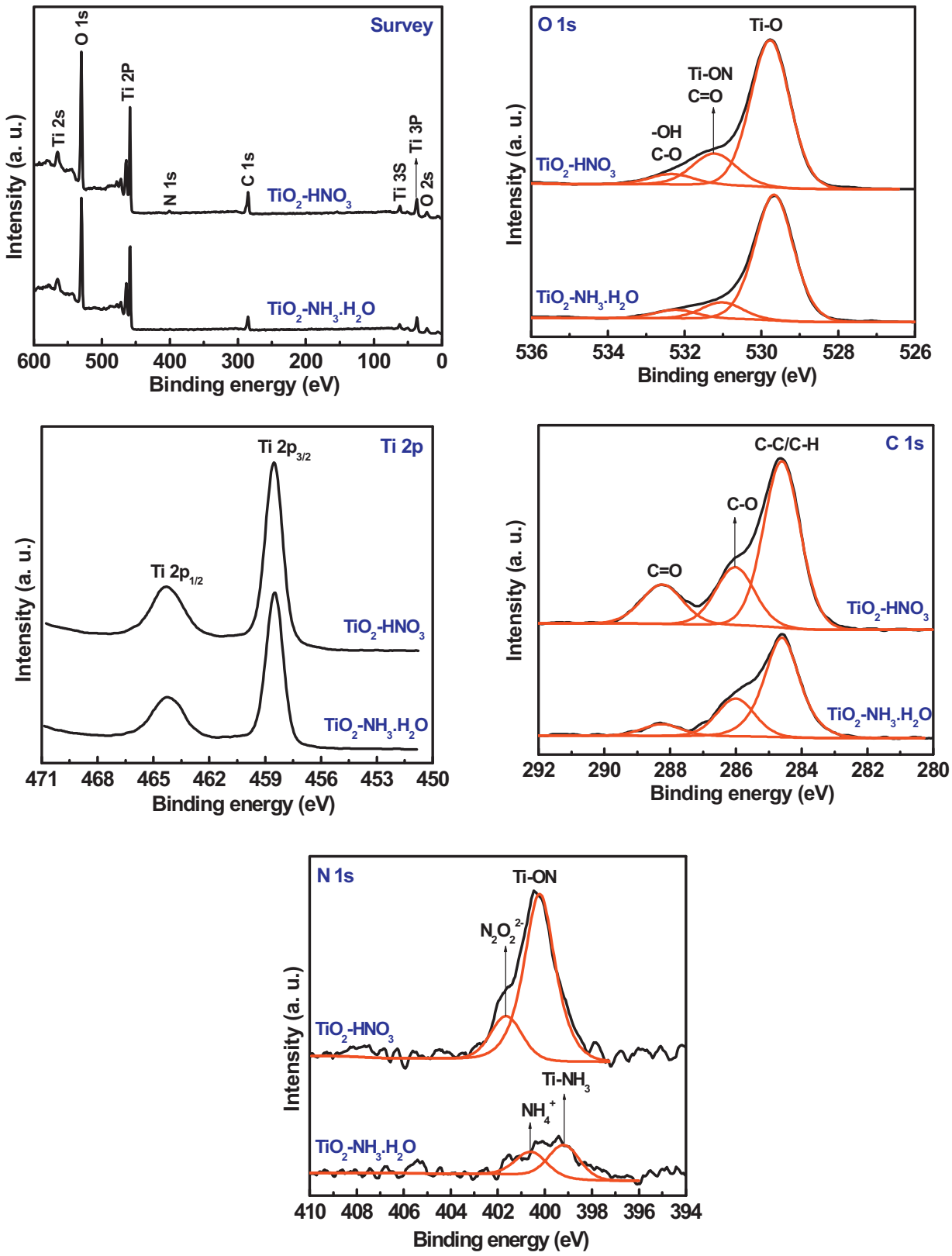

Fig. 3. XPS spectra of TiO_2-$NH_3{\cdot}H_2O$ and TiO_2-HNO_3. (For interpretation of the references to color in this figure legend, the reader is referred to the web version of this article.)

synthesis conditions used [14,19–38,41–49]. Considering the nitrogen sources used in this study (HNO_3 as well as its reduced and thermally decomposed products (e.g., NO species) for TiO_2-HNO_3 and $NH_3{\cdot}H_2O$ for TiO_2-$NH_3{\cdot}H_2O$), solvothermal reaction condition and FTIR results (Fig. 2), we assign the N 1s peaks at 399.2 and 400.2 eV to coordinated NH_3 (Ti-NH_3) and interstitial NO^- (Ti—ON), and the N 1s peaks around 400.6 and 401.6 eV to surface chemisorbed NH_4^+ and $N_2O_2^{2-}$, respectively. Quantification of the N 1s peak areas of the two products reveals that the nitrogen content in TiO_2-HNO_3 is much higher than that in TiO_2-$NH_3{\cdot}H_2O$ (Table 1).

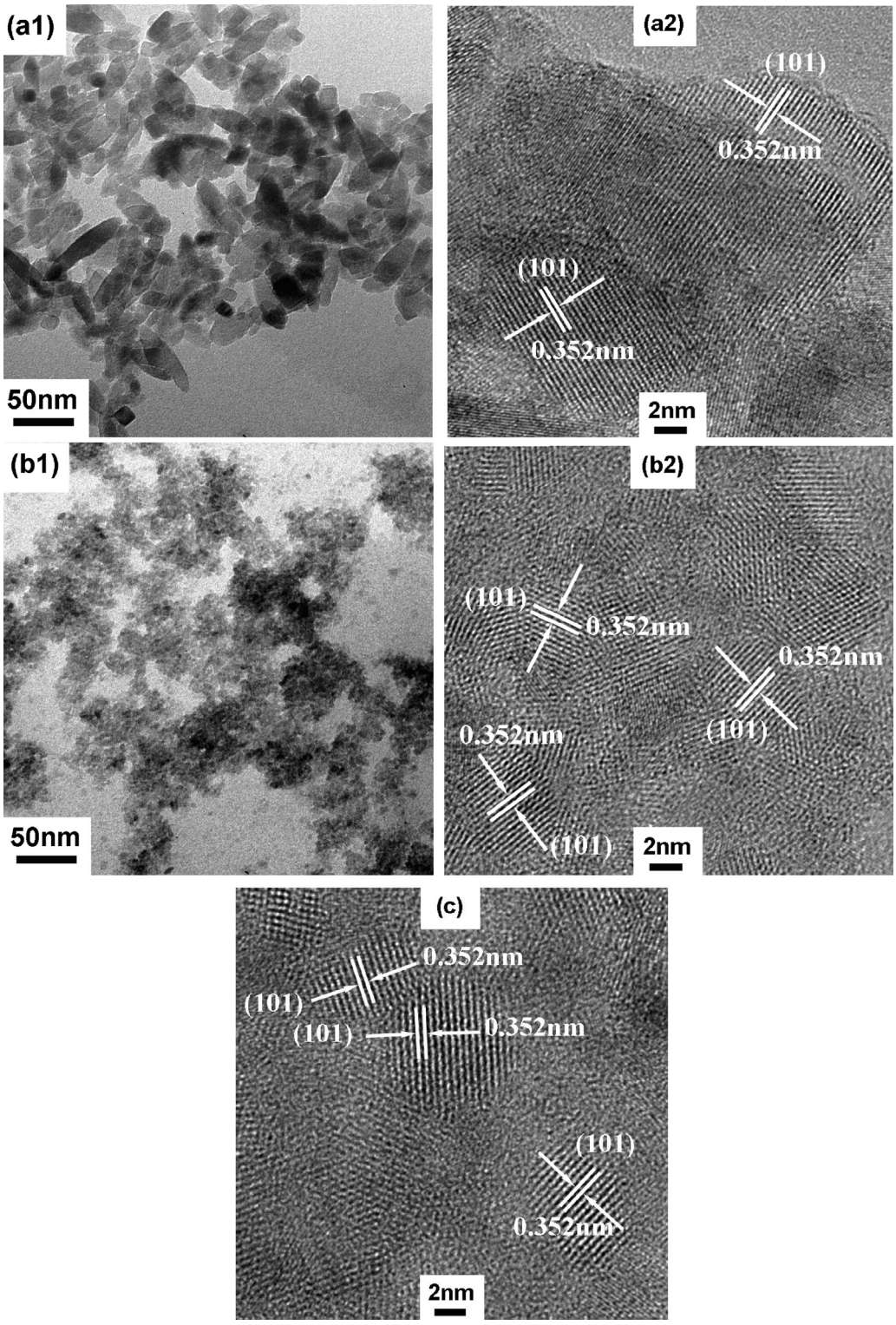

Fig. 4. TEM images of (a1) TiO_2-$NH_3{\cdot}H_2O$ and (b1) TiO_2-HNO_3, and HRTEM images of (a2) TiO_2-$NH_3{\cdot}H_2O$, (b2) TiO_2-HNO_3 and (c) TiO_2-HNO_3-AU.

The TEM and HRTEM images of TiO_2-$NH_3{\cdot}H_2O$ and TiO_2-HNO_3 are shown in Fig. 4(a1) and (a2) and (b1) and (b2), respectively. As can be seen from Fig. 4(a1) and (b1), TiO_2-$NH_3{\cdot}H_2O$ comprises mostly elongated nanoparticles with diameters of about 14–18 nm, whereas TiO_2-HNO_3 comprises much smaller (about 4–6 nm) nanoparticles which are more aggregated due to their higher surface energy. The particle diameters of TiO_2-HNO_3 and TiO_2-$NH_3{\cdot}H_2O$ estimated from their TEM images are in agreement with those derived from the Scherrer formula. Besides, both products display clear lattice fringes in their HRTEM images (Fig. 4(a2) and (b2)), suggesting their high crystallinity. The fringe intervals of 0.352 nm seen in both the HRTEM images of TiO_2-$NH_3{\cdot}H_2O$ and TiO_2-HNO_3 correspond to the interplanar spacing of (1 0 1) crystal planes of anatase TiO_2, and no fringe intervals corresponding to brookite and rutile TiO_2 can be identified, consistent with the XRD results of Fig. 1.

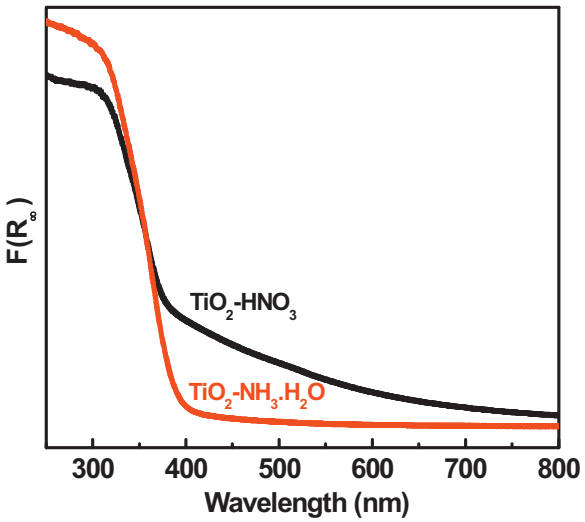

Fig. 5. UV–vis diffuse reflectance spectra of TiO_2-NH_3·H_2O and TiO_2-HNO_3. (For interpretation of the references to color in this figure legend, the reader is referred to the web version of this article.)

The BET specific surface areas of TiO_2-NH_3·H_2O and TiO_2-HNO_3 were determined by N_2 adsorption–desorption isotherms. The obtained results (Table 1) show that the BET specific surface area (208.1 m^2/g) of TiO_2-HNO_3 is much larger than that (87.1 m^2/g) of TiO_2-NH_3·H_2O, which is expected from its smaller crystallite sizes and suggests its more catalytic active surface sites per unit catalyst mass.

The UV–vis diffuse reflectance spectra of TiO_2-NH_3·H_2O and TiO_2-HNO_3 were measured and converted into the absorption mode (Fig. 5) using the Kubelka–Munk function [50–53]:

$$F(R_\infty) = \frac{(1-R_\infty)^2}{2R_\infty} = \frac{\alpha}{S}$$

$$R_\infty = \frac{R_{sample}}{R_{BaSO_4}}$$

where $F(R_\infty)$, R, α and S are the Kubelka–Munk function, reflectance, absorption coefficient and scattering coefficient, respectively. As can be seen from Fig. 5, TiO_2-NH_3·H_2O exhibits a band edge absorption at around 390 nm, but with little absorption of visible light. However, for TiO_2-HNO_3, besides a band edge absorption at around 390 nm, it displays also a distinct tailing absorption covering the whole visible region, which is the typical photoabsorption feature reported for N-doped TiO_2 [19–38,42–45], and suggests TiO_2-HNO_3 has the potential to be a visible light-driven photocatalyst.

Fig. 6 shows the variation of Cr(VI) concentration (initially 50 mg/L) with irradiation time in the presence of 0.4 g of TiO_2-HNO_3, TiO_2-NH_3·H_2O and TiO_2 P25 under UV and visible light ($\lambda > 420$ nm) irradiation, together with the results from the blank experiments (no photocatalyst, but with UV or visible light irradiation). As can be seen from Fig. 6, in the blank experiments, the concentration of Cr(VI) aqueous solution remained constant upon irradiation by UV light for 50 min or visible light ($\lambda > 420$ nm) for 100 min. In the presence of TiO_2-NH_3·H_2O, the concentration of Cr(VI) aqueous solution decreased slowly under UV light irradiation, and much more slowly under visible light irradiation (e.g., only 17% and 7% decrease in the concentration of Cr(VI) aqueous solution upon irradiation by UV light for 50 min and visible light for 100 min, respectively). In the presence of TiO_2 P25, the concentration of Cr(VI) aqueous solution also decreased slowly under UV light irradiation (e.g., only 24% decrease in the concentration of Cr(VI) aqueous solution after UV light irradiation for 50 min), but hardly changed

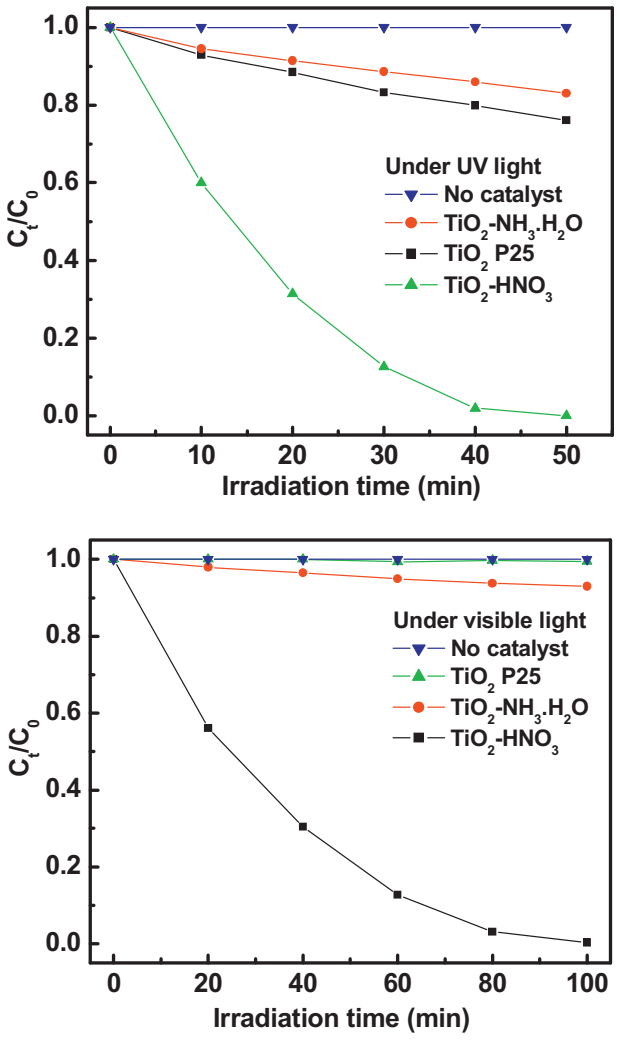

Fig. 6. Variation of Cr(VI) concentration (initial 50 mg/L) with irradiation time in the presence of 0.4 g of TiO_2-HNO_3, TiO_2-NH_3·H_2O and TiO_2 P25 under UV and visible light ($\lambda > 420$ nm) irradiation, together with the results from the blank experiments (no photocatalyst, but with UV or visible light irradiation). *Note*: C_0 and C are the concentrations of Cr(VI) aqueous solution when irradiated for 0 (i.e., just after the dark adsorption) and t min, respectively.

under visible light irradiation for 100 min. In contrast, in the presence of TiO_2-HNO_3, the concentration of Cr(VI) aqueous solution decreased quickly under both UV and visible light ($\lambda > 420$ nm) irradiation, e.g., the concentration of Cr(VI) aqueous solution had decreased to almost zero upon UV irradiation for 50 min or visible light ($\lambda > 420$ nm) irradiation for 100 min. Since the dark adsorption time adopted in this study was 60 min which should be enough to ensure the adsorption–desorption (as well as the chemical reactions, if any) equilibrium between photocatalysts and Cr(VI) in aqueous solution before the photocatalytic experiments (Fig. S3), the quick decrease of Cr(VI) concentration in the presence of TiO_2-HNO_3 under both UV and visible light ($\lambda > 420$ nm) irradiation should be attributed to photocatalytic reduction. Therefore, the results presented in Fig. 6 suggest that TiO_2-HNO_3 possesses much higher photocatalytic activity than TiO_2-NH_3·H_2O and TiO_2 P25 in the reduction of aqueous Cr(VI) under both UV and visible light ($\lambda > 420$ nm) irradiation.

As for the difference in the photocatalytic activities of TiO_2-HNO_3, TiO_2-NH_3·H_2O and TiO_2 P25, it is most likely an outcome of the combined action of many factors, such as composition, phase, photoabsorption, adsorption capacity for Cr(VI), specific surface

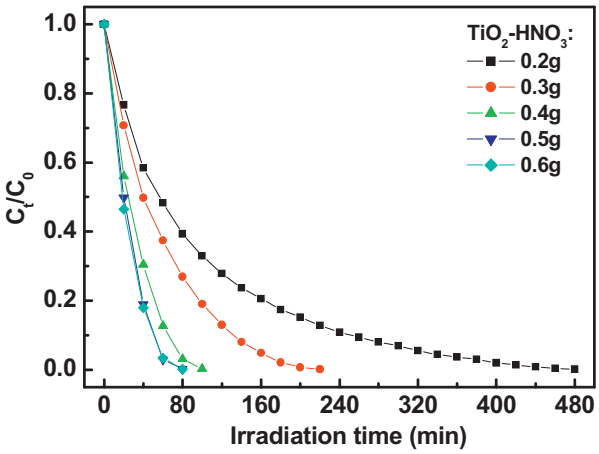

Fig. 7. Effect of the dosage of TiO_2-HNO_3 on photocatalytic reduction of 50 mg/L Cr(VI) under visible light (λ > 420 nm) irradiation.

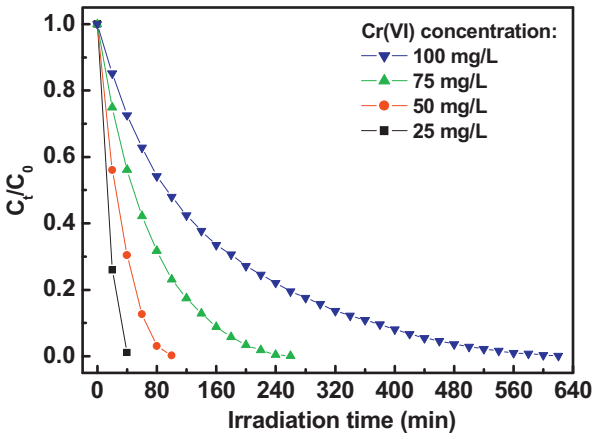

Fig. 8. Effect of the initial concentration of Cr(VI) aqueous solution on photocatalytic reduction of Cr(VI) over 0.4 g of TiO_2-HNO_3 under visible light (λ > 420 nm) irradiation.

area, size, crystallinity, surface states and crystal defects. However, considering their physicochemical characteristics (Table 1) and Fig. 5, it is believed that the wide visible spectrum response, larger specific surface area and smaller crystallite size of TiO_2-HNO_3 should contribute to its exceptionally higher photocatalytic activity under visible light (λ > 420 nm) [37,38], whereas the larger specific surface area and smaller crystallite size of TiO_2-HNO_3 should play predominant roles in its much higher photocatalytic activity under UV light, as compared with TiO_2-$NH_3{\cdot}H_2O$ and TiO_2 P25.

Fig. 7 shows the effect of the dosage of TiO_2-HNO_3 on photocatalytic reduction of 50 mg/L Cr(VI) under visible light (λ > 420 nm) irradiation. As can be seen from Fig. 7, the increase of the dosage of TiO_2-HNO_3 (while the other conditions are the same) from 0.2 to 0.5 g can shorten the irradiation time needed for the complete reduction of 50 mg/L Cr(VI) (it was also noticed that the irradiation time needed for the complete reduction of 50 mg/L Cr(VI) was shortened much more for each 0.1 g increase of TiO_2-HNO_3 from 0.2 to 0.4 g than from 0.4 to 0.5 g), but further increase of the dosage of TiO_2-HNO_3 from 0.5 to 0.6 g cannot shorten the irradiation time needed for the complete reduction of 50 mg/L Cr(VI), e.g., the irradiation times needed for the complete reduction of 50 mg/L Cr(VI) in the presence of 0.2, 0.3, 0.4, 0.5 and 0.6 g of TiO_2-HNO_3 were in turn 480, 220, 100, 80 and 80 min. To quantitatively compare the photocatalytic reduction of Cr(VI) over TiO_2-HNO_3 under different conditions (e.g., different dosages of TiO_2-HNO_3 and different initial concentrations of Cr(VI) aqueous solution), we introduced "the efficiency of Cr(VI) reduction", which was defined as "(initial Cr(VI) concentration)/(dosage of TiO_2-HNO_3 × irradiation time used for the complete reduction of Cr(VI))". Thus, for 50 mg/L Cr(VI), the efficiencies of Cr(VI) reduction in the presence of 0.2, 0.3, 0.4, 0.5 and 0.6 g of TiO_2-HNO_3 were calculated to be 0.52, 0.76, 1.25, 1.25 and 1.04 mg/L g^{-1} min^{-1}, respectively. Obviously, the enhancement in the efficiency of Cr(VI) reduction was quite significant, when the dosage of TiO_2-HNO_3 was increased from 0.2 to 0.4 g. The efficiency of Cr(VI) reduction reached the maximum when the dosages of TiO_2-HNO_3 were 0.4 and 0.5 g. Further increase of the dosage of TiO_2-HNO_3 from 0.5 to 0.6 g, the efficiencies of Cr(VI) reduction began to decline. Such phenomena are characteristic of heterogeneous catalysis, and can be rationalized in terms of the availability of the surface active sites of photocatalyst and the penetration of the incident visible light into the suspension [54–58]. With increase of the photocatalyst dosage (while the other conditions are the same), on one hand, the surface active sites of photocatalyst available for adsorption, photoabsorption and subsequent photocatalytic reactions increase, which can accelerate the rate of photocatalytic reactions; on the other hand, the light-blocking effect of photocatalyst also increases and accordingly the penetration of the incident visible light into the suspension decreases, which result in decreased illuminated volume of the suspension and lower photocatalytic efficiencies [54–58]. These two opposite effects of the photocatalyst dosage suggest there always exists a optimum dosage of photocatalyst (e.g., 0.4 g of TiO_2-HNO_3 for 50 mg/L Cr(VI) in this study) to achieve the highest efficiency of Cr(VI) reduction.

Fig. 8 shows the effect of initial concentration of Cr(VI) aqueous solution on photocatalytic reduction of Cr(VI) over 0.4 g of TiO_2-HNO_3 under visible light (λ > 420 nm) irradiation. It can be seen from Fig. 8 that at the same dosage (0.4 g) of TiO_2-HNO_3, the irradiation time needed for the complete reduction of Cr(VI) increased with the increase of initial Cr(VI) concentration, e.g., the irradiation times needed for the complete reduction of 25, 50, 75 and 100 mg/L Cr(VI) were 40, 100, 260 and 620 min, respectively. For 25, 50, 75 and 100 mg/L Cr(VI), the efficiencies of Cr(VI) reduction over 0.4 g of TiO_2-HNO_3 can be calculated to be 1.56, 1.25, 0.72 and 0.40 mg/L g^{-1} min^{-1}, respectively. The decrease of the efficiencies of Cr(VI) reduction with the increase of initial Cr(VI) concentration can be explained mainly from the following two aspects [55–58]: first, the surface active sites of 0.4 g of TiO_2-HNO_3 are limited, so more Cr(VI) will remain in the solution at higher initial Cr(VI) concentrations, but the Cr(VI) remained in the solution cannot be reduced because photocatalytic reduction of Cr(VI) typically occurs on the surface of photocatalyst; second, higher concentration of Cr(VI) aqueous solution can absorb more of the incident visible light with wavelengths in the range of about 420–480 nm (Fig. S4), thus decreasing the penetration of the latter into the former as well as the photon flux received by TiO_2-HNO_3.

The recovered TiO_2-HNO_3 after use in the photocatalytic reduction of Cr(VI) (TiO_2-HNO_3-AU) was further characterized by means of XRD, HRTEM and XPS. The XRD pattern (Fig. 1(c)) and HRTEM image (Fig. 4(c)) of TiO_2-HNO_3-AU resemble those (Figs. 1(b) and 4(b2)) of the fresh TiO_2-HNO_3, manifesting its anatase structure. The survey XPS spectrum of TiO_2-HNO_3-AU (Fig. 9) reveals the presence of Ti, O, N, C and Cr elements. The binding energies of Ti $2p_{3/2}$, O 1s, N 1s and C 1s of TiO_2-HNO_3-AU are in turn 458.5, (529.8, 531.3 and 532.7), (400.3 and 401.5) and (284.6, 286.0 and 288.2) eV (Fig. 9), which are in agreement with those of the fresh TiO_2-HNO_3 (Fig. 3). Thus, the above XRD, HRTEM and XPS results indicate that anatase N-doped TiO_2 is still maintained after the photocatalytic use. As for the Cr deposit on TiO_2-HNO_3-AU, the binding energies of Cr $2p_{3/2}$ and Cr $2p_{1/2}$ are observed at about 577.2 and 586.1 eV (Fig. 9), respectively, which correspond to Cr(III) [46,59–65]. In addition, the green surface color

of TiO_2-HNO_3-AU also suggests the presence of Cr(III). Therefore, it can be concluded that Cr(VI) is reduced to Cr(III) after the TiO_2-HNO_3-mediated photocatalytic reactions.

There is now a general consensus that the doping of TiO_2 with nitrogen at the interstitial sites would create intra-bandgap states about 0.7–0.8 eV above the valence band (VB) edge [66,67], which are responsible for the absorption of visible light. A smaller fraction of the intra-bandgap states bear one electron in the singly occupied molecular orbital and are consequently paramagnetic (NO^{2-}), whereas the others are diamagnetic with two electrons in the highest occupied molecular orbital (NO^{3-}) [66,67]. Nevertheless, the positions of the conduction band and valence band of TiO_2 would remain almost unchanged upon nitrogen doping [66,67]. Under UV light irradiation, the electrons in the VB of TiO_2-HNO_3 can be directly excited to its CB, simultaneously leaving behind an equal amount of electron vacancies or "holes" in its VB, thus forming the electron–hole pairs. Under visible light ($\lambda > 420$ nm) irradiation, the electrons in the VB of TiO_2-HNO_3 cannot be directly (single-step) excited to its CB. But the existence of NO^{2-} and NO^{3-} intra-bandgap states allows TiO_2-HNO_3 to absorb the needed photon energy for moving electrons from VB to CB via two different steps of electron excitation, i.e., the electron excitation from NO^{3-} to CB ($NO^{3-} - e^- = NO^{2-}$) and from VB to NO^{2-} ($NO^{2-} + e^- = NO^{3-}$) [66], in which the NO^{2-} and NO^{3-} intra-bandgap states play a role of electron transfer intermediate or "stepping-stone". Therefore, the charge carrier formation/separation can also be realized by $\lambda > 420$ nm light irradiation of TiO_2-HNO_3. A portion of the photogenerated electrons and holes migrate to the photocatalyst surface and participate in reduction and oxidation reactions, respectively, with adsorbed species, i.e., the photogenerated electrons (e^-) reduce Cr(VI) to Cr(III); concomitantly, the photogenerated holes (h^+) oxidize H_2O to O_2 [17]. The schematic diagram for TiO_2-HNO_3-mediated photocatalytic reduction of Cr(VI) in water under both UV and visible light irradiation is shown in Scheme 1.

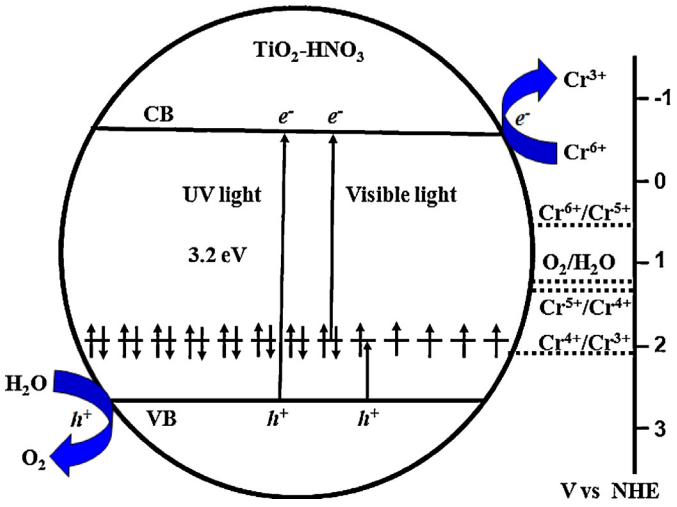

Scheme 1. Schematic diagram for TiO_2-HNO_3-mediated photocatalytic reduction of Cr(VI) in water. *Note*: the standard reduction potentials of the likely involved Cr(VI)/Cr(V), Cr(V)/Cr(IV), Cr(IV)/Cr(III) and O_2/H_2O redox couples are in turn 0.55, 1.34, 2.10 and 1.229 V (vs NHE) [71,74].

Previous works have shown that the semiconductor-mediated photocatalytic reduction of Cr(VI) under normal illuminations (not intense laser irradiation) takes place through three consecutive one-electron transfer steps [68–71], ending in Cr(III) [59–65,68–71]. The first electron transfer step ($Cr(VI) + e_{CB}^- = Cr(V)$) was usually considered as the rate-determining one [71]. To realize heterogeneous photocatalytic reduction of Cr(VI), the bottom level of the conduction band of the adopted semiconductor photocatalyst should be more negative than the reduction potential of Cr(VI)/Cr(V), 0.55 V (vs NHE) [71]. Since nitrogen doping cannot significantly alter the conduction

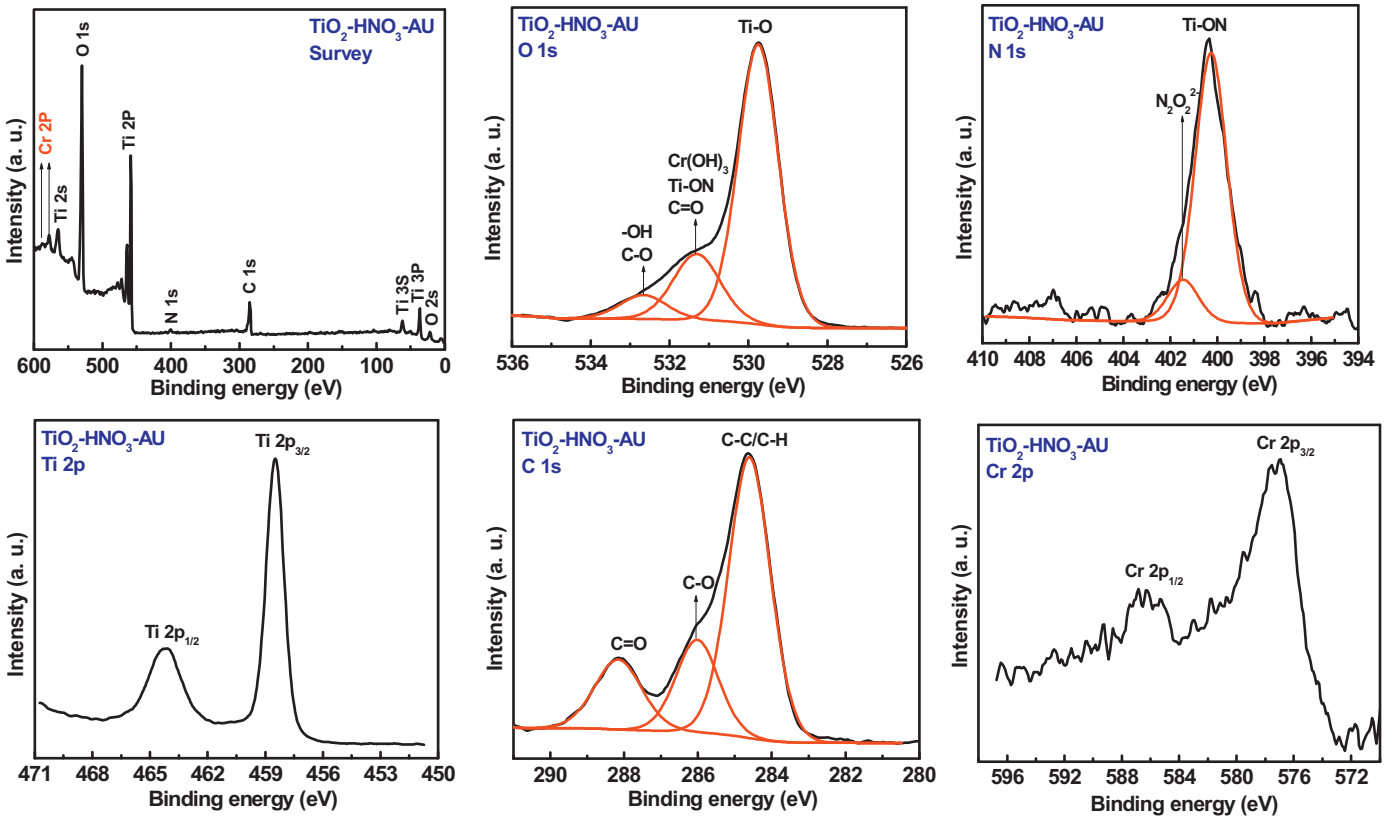

Fig. 9. XPS spectra of TiO_2-HNO_3-AU. (For interpretation of the references to color in this figure legend, the reader is referred to the web version of this article.)

band position of TiO_2 [66,67], the conduction band potential of N-doped TiO_2 (e.g., TiO_2-HNO_3 in this study) can be estimated in the same way as for undoped TiO_2: the conduction band potential of anatase TiO_2 at 25 °C = −0.23 V − 0.059 V × pH value (vs NHE) [72,73]. Consequently, the conduction band potential of TiO_2-HNO_3 at pH = 5.2 can be estimated to be −0.537 V (vs NHE). Because the conduction band potential of TiO_2-HNO_3 is more negative than the reduction potential of Cr(VI)/Cr(V), the photocatalytic reduction of Cr(VI) over TiO_2-HNO_3 is thermodynamically favorable. This is consistent with our photocatalytic results.

4. Conclusions

N-doped TiO_2 nanocrystals with high specific surface area and remarkable visible light absorption were successfully synthesized by our proposed one-step low temperature (180 °C) solvothermal route, which adopted HNO_3 as the nitrogen source. Our proposed method is simple, performed at low temperature and using only common and inexpensive reactants, thus providing a viable strategy for synthesizing multifunctional N-doped TiO_2 nanomaterials.

Through the photocatalytic experiments using Cr(VI) as a probe contaminant, the following results were obtained: (1) TiO_2-HNO_3 possesses exceptionally higher photocatalytic activity than TiO_2-$NH_3{\cdot}H_2O$ and TiO_2 P25 in the reduction of Cr(VI) in water under both UV and visible light ($\lambda > 420$ nm) irradiation; (2) the dosage of TiO_2-HNO_3 and the initial concentration of Cr(VI) aqueous solution significantly affect the efficiency of Cr(VI) reduction; and (3) Cr(VI) is reduced to Cr(III). The outstanding photocatalytic performance of TiO_2-HNO_3 renders it a promising photocatalyst in efficient utilization of solar energy for Cr(VI) wastewater treatment.

Acknowledgements

Dr. Dionysiou acknowledges support from the National Science Foundation (US-Ireland collaborative research CBET) (1033317) for his involvement on this project. This is also a project funded by the Priority Academic Program Development of Jiangsu Higher Education Institutions, China Scholarship Council (CSC) Scholarships (2011832350), and the Science & Technology Innovation Fund of Yangzhou University (2012CXJ017). Also, thanks to The Testing Center of Yangzhou University for the characterization data.

Appendix A. Supplementary data

Supplementary data associated with this article can be found, in the online version, at http://dx.doi.org/10.1016/j.apcatb.2013.05.023.

References

[1] A. Kleiman, A. Márquez, M.L. Vera, J.M. Meichtry, M.I. Litter, Applied Catalysis B 101 (2011) 676–681.
[2] M.V. Dozzi, A. Saccomanni, E. Selli, Journal of Hazardous Materials 211/212 (2012) 188–195.
[3] Y.C. Zhang, J. Li, M. Zhang, D.D. Dionysiou, Environmental Science and Technology 45 (2011) 9324–9331.
[4] L. Yang, Y. Xiao, S. Liu, Y. Li, Q. Cai, S. Luo, G. Zeng, Applied Catalysis B 94 (2010) 142–149.
[5] S. Luo, Y. Xiao, L. Yang, C. Liu, F. Su, Y. Li, Separation and Purification Technology 79 (2011) 85–91.
[6] P.S. Suchithra, C.P. Shadiya, A. Peer Mohamed, P. Velusamy, S. Ananthakumar, Applied Catalysis B 130 (131) (2013) 44–53.
[7] S.K. Choi, H.S. Yang, J.H. Kim, H. Park, Applied Catalysis B 121 (122) (2012) 206–213.
[8] X. An, J.C. Yu, F. Wang, C. Li, Y. Li, Applied Catalysis B 129 (2013) 80–88.
[9] S. Liu, N. Zhang, Z.R. Tang, Y.J. Xu, ACS Applied Materials and Interfaces 4 (2012) 6378–6385.
[10] G. Chen, M. Sun, Q. Wei, Z. Ma, B. Du, Applied Catalysis B 125 (2012) 282–287.
[11] H. Ma, J. Shen, M. Shi, X. Lu, Z. Li, Y. Long, Applied Catalysis B 121 (122) (2012) 198–205.
[12] H. Chen, Y. Shao, Z. Xu, H. Wan, Y. Wan, S. Zheng, Applied Catalysis B 105 (2011) 255–262.
[13] C.E. Barrera-Díaz, V. Lugo-Lugo, B. Bilyeu, Journal of Hazardous Materials 223 (224) (2012) 1–12.
[14] M. Pelaez, N.T. Nolan, S.C. Pillai, M.K. Seery, P. Falaras, A.G. Kontos, P.S.M. Dunlop, J.W.J. Hamilton, J.A. Byrne, K. O'Shea, M.H. Entezari, D.D. Dionysiou, Applied Catalysis B 125 (2012) 331–349.
[15] E. Casbeer, V.K. Sharma, X.Z. Li, Separation and Purification Technology 87 (2012) 1–14.
[16] H.T. Hsu, S.S. Chen, Y.S. Chen, Separation and Purification Technology 80 (2011) 663–669.
[17] Q. Wang, C. Chen, W. Ma, H. Zhu, J. Zhao, Chemistry – A European Journal 15 (2009) 4765–4769.
[18] A.E. Giannakas, E. Seristatidou, Y. Deligiannakis, I. Konstantinou, Applied Catalysis B 132 (133) (2013) 460–468.
[19] N.T. Nolan, D.W. Synnott, M.K. Seery, S.J. Hinder, A.V. Wassenhoven, S.C. Pillai, Journal of Hazardous Materials 211 (212) (2012) 88–94.
[20] G.B. Soares, B. Bravin, C.M.P. Vaz, C. Ribeiro, Applied Catalysis B 106 (2011) 287–294.
[21] J. Lu, L. Li, Z. Wang, B. Wen, J. Cao, Materials Letters 94 (2013) 147–149.
[22] H. Diker, C. Varlikli, K. Mizrak, A. Dana, Energy 36 (2011) 1243–1254.
[23] Y. Wang, C. Feng, M. Zhang, J. Yang, Z. Zhang, Applied Catalysis B 104 (2011) 268–274.
[24] P. Zhang, S. Yin, T. Sato, Applied Catalysis B 103 (2011) 462–469.
[25] M. D'Arienzo, R. Scotti, L. Wahba, C. Battocchio, E. Bemporad, A. Nale, Applied Catalysis B 93 (2009) 149–155.
[26] T. Sano, N. Mera, Y. Kanai, C. Nishimoto, S. Tsutsui, T. Hirakawa, Applied Catalysis B 128 (2012) 77–83.
[27] P.S. Yap, T.T. Lim, Applied Catalysis B 101 (2011) 709–717.
[28] D. Huang, Y. Miyamoto, J. Ding, J. Gu, S. Zhu, Q. Liu, T. Fan, Q. Guo, D. Zhang, Materials Letters 65 (2011) 326–328.
[29] A. Kubacka, B. Bachiller-Baeza, G. Colón, M. Fernández-García, Applied Catalysis B 93 (2010) 274–281.
[30] R. Jaiswal, N. Patel, D.C. Kothari, A. Miotello, Applied Catalysis B 126 (2012) 47–54.
[31] X. Wang, T.T. Lim, Applied Catalysis B 100 (2010) 355–364.
[32] Y. Cong, B. Tian, J. Zhang, Applied Catalysis B 101 (2011) 376–381.
[33] S.S. Thind, G. Wu, A. Chen, Applied Catalysis B 111/112 (2012) 38–45.
[34] D.P. Subagio, M. Srinivasan, M. Lim, T.T. Lim, Applied Catalysis B 95 (2010) 414–422.
[35] Z. He, W. Que, J. Chen, X. Yin, Y. He, J. Ren, ACS Applied Materials and Interfaces 4 (2012) 6816–6826.
[36] D. Dolat, N. Quici, E. Kusiak-Nejman, A.W. Morawski, G.L. Puma, Applied Catalysis B 115/116 (2012) 81–89.
[37] H. Li, J. Li, Y. Huo, Journal of Physical Chemistry B 110 (2006) 1559–1565.
[38] Y. Huo, Y. Jin, J. Zhu, H. Li, Applied Catalysis B 89 (2009) 543–550.
[39] C.J. Li, G.R. Xu, Applied Surface Science 257 (2011) 4951–4955.
[40] K. Hadjiivanov, H. Knözinger, Physical Chemistry Chemical Physics 2 (2000) 2803–2806.
[41] M.J. Velasco, F. Rubio, J. Rubio, J.L. Oteo, Thermochimica Acta 326 (1999) 91–97.
[42] X. Chen, X. Wang, Y. Hou, J. Huang, L. Wu, X. Fu, Journal of Catalysis 255 (2008) 59–67.
[43] Z. Ai, L. Zhu, S. Lee, L. Zhang, Journal of Hazardous Materials 192 (2011) 361–367.
[44] L. Gai, Q. Mei, X. Duan, H. Jiang, G. Zhou, Journal of Solid State Chemistry 199 (2013) 271–279.
[45] F. Peng, L. Cai, H. Yu, H. Wang, J. Yang, Journal of Solid State Chemistry 181 (2008) 130–136.
[46] J.F. Moulder, W.F. Stickle, P.E. Sobol, K.D. Bomben, in: J. Chastain (Ed.), Handbook of X-ray Photoelectron Spectroscopy, Perkin-Elmer Corp., Eden Prairie, 1992.
[47] F. Spadavecchia, G. Cappelletti, S. Ardizzone, C.L. Bianchi, S. Cappelli, C. Oliva, Applied Catalysis B 96 (2010) 314–322.
[48] S.H. Lee, E. Yamasue, K.N. Ishihara, H. Okumura, Applied Catalysis B 93 (2010) 217–226.
[49] Y.P. Peng, E. Yassitepe, Y.T. Yeh, I. Ruzybayev, S.I. Shah, C.P. Huang, Applied Catalysis B 125 (2012) 465–472.
[50] Y.C. Zhang, Z.N. Du, K.W. Li, M. Zhang, D.D. Dionysiou, ACS Applied Materials and Interfaces 3 (2011) 1528–1537.
[51] Y.C. Zhang, Z.N. Du, K.W. Li, M. Zhang, Separation and Purification Technology 81 (2011) 101–107.
[52] W. Shi, N. Chopra, ACS Applied Materials and Interfaces 4 (2012) 5590–5607.
[53] V. Nadtochenko, N. Denisov, A. Gorenberg, Yu Kozlov, P. Chubukov, J.A. Rengifo, Applied Catalysis B 91 (2009) 460–469.
[54] Y.C. Zhang, Z.N. Du, S.Y. Li, M. Zhang, Applied Catalysis B 95 (2010) 153–159.
[55] K. Vignesh, R. Priyanka, M. Rajarajan, A. Suganthi, Materials Science and Engineering B 178 (2013) 149–157.
[56] H. Mekatel, S. Amokrane, B. Bellal, M. Trari, D. Nibou, Chemistry – A European Journal 200 (202) (2012) 611–618.
[57] M. Qamar, M.A. Gondal, Z.H. Yamani, Journal of Hazardous Materials 187 (2011) 258–263.
[58] A. Idris, N. Hassan, R. Rashid, A.-F. Ngomsik, Journal of Hazardous Materials 186 (2011) 629–635.
[59] N. Wang, Y. Xu, L. Zhu, X. Shen, H. Tang, Journal of Photochemistry and Photobiology A 201 (2009) 121–127.
[60] X. Liu, H. Bai, Powder Technology 237 (2013) 610–615.
[61] J. Li, T. Wang, X. Du, Separation and Purification Technology 101 (2012) 11–17.

[62] T.X. Wang, S.H. Xu, F.X. Yang, Materials Letters 83 (2012) 46–48.
[63] Y.C. Zhang, J. Li, H.Y. Xu, Applied Catalysis B 123 (124) (2012) 18–26.
[64] L. Wang, X. Li, W. Teng, Q. Zhao, Y. Shi, R. Yue, Journal of Hazardous Materials 244 (245) (2013) 681–688.
[65] S.C. Xu, Y.X. Zhang, S.S. Pan, H.L. Ding, G.H. Li, Journal of Hazardous Materials 196 (2011) 29–35.
[66] G. Barolo, S. Livraghi, M. Chiesa, M.C. Paganini, E. Giamello, Journal of Physical Chemistry C 116 (2012) 20887–20894.
[67] C.D. Valentin, E. Finazzi, G. Pacchioni, A. Selloni, S. Livraghi, M.C. Paganini, E. Giamello, Chemical Physics 339 (2007) 44–56.
[68] J.J. Testa, M.A. Grela, M.I. Litter, Langmuir 17 (2001) 3515–3517.
[69] J.M. Meichtry, M. Brusa, G. Mailhot, M.A. Grela, M.I. Litter, Applied Catalysis B 71 (2007) 101–107.
[70] J.J. Testa, M.A. Grela, M.I. Litter, Environmental Science and Technology 38 (2004) 1589–1594.
[71] M.I. Litter, Advanced Chemical Engineering 36 (2009) 37–67.
[72] T. Papadam, N.P. Xekoukoulotakis, I. Poulios, D. Mantzavinos, Journal of Photochemistry and Photobiology A 186 (2007) 308–315.
[73] N. Wang, L. Zhu, K. Deng, Y. She, Y. Yu, H. Tang, Applied Catalysis B 95 (2010) 400–407.
[74] X. Mao, A. Ciblak, M. Amiri, A.N. Alshawabkeh, Environmental Science and Technology 45 (2011) 6517–6523.